

# Impact of varying atmospheric profiles on extensive air shower observation: Fluorescence light emission and energy reconstruction

B. Keilhauer <sup>a,\*</sup>, J. Blümer <sup>a,b</sup>, R. Engel <sup>b</sup>, H.O. Klages <sup>b</sup>

<sup>a</sup> *Institut für Experimentelle Kernphysik, Universität Karlsruhe, Postfach 3640, 76021 Karlsruhe, Germany*

<sup>b</sup> *Forschungszentrum Karlsruhe, Institut für Kernphysik, Postfach 3640, 76021 Karlsruhe, Germany*

Received 4 November 2005; received in revised form 17 February 2006; accepted 20 February 2006

Available online 20 March 2006

## Abstract

Several experiments measure the fluorescence light produced by extensive air showers in the atmosphere. This light is converted into a longitudinal shower profile from which information on the primary energy and composition is derived. The fluorescence yield, as the conversion factor between light profile measured by EAS experiments and physical interpretation of showers, has been measured in several laboratory experiments. The results, however, differ considerably. In this article, a model calculation of the fluorescence emission from relevant band systems of nitrogen in dependence on wavelength and atmospheric conditions is presented. Different calculations are compared to each other in combination with varying input parameters. The predictions are compared with measurements and the altitude dependence of the fluorescence yield is discussed in detail.

© 2006 Elsevier B.V. All rights reserved.

*PACS:* 96.40.Pq

*Keywords:* Fluorescence light emission; Extensive air shower; Atmosphere

## 1. Introduction

This is the second article of a series of investigations of the importance of atmospheric properties for the reconstruction of extensive air showers (EAS). The first article [1] describes the effect of changing atmospheric density profiles on the longitudinal EAS development. In particular, if the fluorescence technique is applied, the conversion of atmospheric depth, as used in shower simulations, to geometrical altitude, as reconstructed from fluorescence measurements, and vice versa is very important for primary cosmic ray mass reconstruction.

This article addresses the fluorescence light emission of EAS which is used for the determination of the total energy

of EAS. In several air shower experiments, for example, HiRes [2], the Pierre Auger Observatory [3–5], and Telescope Array [6,7], the fluorescence technique is employed for detecting EAS. Measuring the fluorescence light that nitrogen molecules emit after being excited by charged particles traversing the atmosphere is the most direct method of detecting the longitudinal shower profile. For the event reconstruction procedures of these air shower experiments, the knowledge of the fluorescence yield  $FY_\lambda$  and its dependence on atmospheric conditions are crucial parameters.

The Pierre Auger Observatory is up to now the only existing EAS experiment which applies hybrid detection techniques. The secondary particles of an EAS are measured at ground and simultaneously the fluorescence light of the longitudinal shower development is detected with telescopes. For extracting a cosmic ray spectrum from the data, the events detected with ground detectors are analyzed

\* Corresponding author.

*E-mail address:* [bianca.keilhauer@ik.fzk.de](mailto:bianca.keilhauer@ik.fzk.de) (B. Keilhauer).

while the energy calibration is deduced from fluorescence detector events and the correlation of these two types of events is derived from hybrid events [8]. This cosmic ray spectrum and its comparison with spectra published by other experiments (AGASA [9] and HiRes [10], for a recent review see [11]) reveal that the fluorescence yield might be a crucial parameter for the energy reconstruction of air showers. For the conversion of detected fluorescence light to energy deposited in the atmosphere by EAS and finally to the total energy of the primary particle, not only the total fluorescence yield in the detected wavelength ( $\lambda$ ) region is important but also the spectral distribution. For example, the emitted light suffers *Rayleigh* scattering while traversing the atmosphere towards the telescopes. Since the scattering cross-section has a  $\lambda^{-4}$  dependence, the long-wavelength part of the fluorescence spectrum has a higher transmission than the short-wavelength region.

The outline of this paper is as follows. In Section 2, the fluorescence emission in air is reviewed and an analytical model (Section 2.1) for calculating the fluorescence emission in dependence on wavelength and atmospheric conditions is described. Particularly, the band systems of nitrogen contributing mainly to the fluorescence light emission are discussed. A compilation of several parameters from different authors used in calculations of this paper is given in Section 2.2. In Section 3 a detailed comparison of measurements with the calculations is done. The aim is to combine the laboratory measurements with our current understanding of the fluorescence emission processes in the atmosphere, to show possible sources of uncertainty, and to provide an easy way of accounting for varying atmospheric conditions. The dependence on these atmospheric conditions is explicitly presented in Section 4.

## 2. Model for fluorescence light emission in air

The most numerous charged particles in an EAS are electrons and positrons. Their energy deposit in air by ionization and excitation of air molecules gives rise to fluorescence light emission. In the wavelength region between 300 and 400 nm, the band systems with the strongest emissions are found. Therefore, all EAS experiments using the fluorescence technique apply UV filters with largest transmittance between roughly 310 and 400 nm. The residual wavelengths are cut in favor of reducing the night sky background.

The major components of the atmosphere are 78.08%  $N_2$ , 20.95%  $O_2$ , and 0.93% Ar per volume. All three constituent parts influence the emission of fluorescence light, however, with strongly differing importance.

The main fluorescence light is emitted by two electronic states of  $N_2$ , these are the second-positive (2P) band system,  $C^3\Pi_u - B^3\Pi_g$ , and the first-negative (1N) system of  $N_2^+$ ,  $B^2\Sigma_u^+ - X^2\Sigma_g^+$ . Each band within a system belongs to a transition from a vibrational level of the upper state  $v'$  to a vibrational level of the lower state  $v''$  [18]. The band structure is caused by the rotational levels and consists of

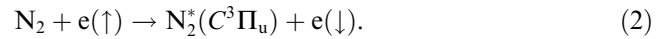
a large number of spectral lines which are very close to each other [19]. These lines will not be distinguished in this work. The bands usually have a *band head* at one end where the intensity falls off suddenly. In the following, the wavelength given for each band belongs to the position of the corresponding band head.

For both, absorption and emission, the *Franck–Condon principle* applies in good approximation. Three processes of excitation of  $N_2$  can be distinguished:

- *Direct excitation:* The energy deposited in air excites nitrogen molecules proportional to an energy-dependent cross-section  $\sigma_{v'}(E)$ . This process mainly acts on the  $N_2^+$  1N system



- *Excitation via secondary electrons:* High energy particles in EAS ionize  $N_2$  producing several lower energy secondary electrons. These  $e^-$  are able to excite also the  $N_2$  2P system with a resultant spin change



In addition, the 2P system can also be excited by recombination



- *Via Auger electrons:* Some ionization processes will release K-electrons leading to the emission of Auger electrons. These are on their part again able to excite the  $N_2$  molecules. However, it must be emphasized that the cross-section for this K-shell ionization is much lower than those for the processes mentioned above. The cross-sections for  $N_2$  excitation and for the ionization to  $N_2^+$  are of the order of  $10^{-21} \text{ m}^2$  [20,21] and for the K-shell ionization of the order of  $10^{-23} \text{ m}^2$  [22].

In air, the optical emission of the prompt radiative return from the upper states of the 2P and 1N system of nitrogen will be affected by some competing processes. The most important process is collisional quenching. Excited nitrogen molecules might collide with other molecules in air before the de-excitation via fluorescence light emission happens.

Argon can be excited by the reaction  $e + \text{Ar} \rightarrow \text{Ar}^*$ , where the excitation cross-section is largest for  $\text{Ar}(^3P_2)$  [12]. This process is followed by  $\text{Ar}^* + N_2 \rightarrow \text{Ar} + N_2^*(C^3\Pi_u)$ . The energy is mainly transferred from argon to nitrogen via secondary electrons rather than direct collisions [13]. The excited state  $C^3\Pi_u$  is the upper level of the second-positive (2P) system of  $N_2$  which radiates photons mainly in the wavelength region between 300 and 400 nm. The lower state is  $B^3\Pi_g$ . This increase of the emission competes, however, with a higher quenching rate, which leads to non-radiative de-excitation, due to additional collision partners in the form of argon atoms in air. The net effect of argon is expected to be less than 1% contribution to the fluorescence light [14]. However, argon

emits also directly fluorescence light at around 310 nm [15]. This transition,  $A^2\Sigma^+ - X^2\Pi$ , has been investigated in argon water–vapor mixtures and the highest intensity has been found for very low argon pressure and 0.06 hPa water vapor. For EAS experiments, this contributions will be of minor importance, too.

The UV–fluorescence light emission from  $O_2$  is negligible [16]. The contribution in the relevant wavelength region stems from  $O_2^+ A^2\Pi_u - X^2\Pi_g$  transmissions. However, already the *Einstein coefficients*<sup>1</sup> are reduced in average by a factor of about 30 compared to the emissions of the 2P system of  $N_2$  [17]. The emissions of atomic oxygen start at 395 nm and go up to 845 nm [16]. These bands are of no importance for EAS experiments.

Generally, it is assumed that the fluorescence light is proportional to the energy deposit of an EAS. The contribution of electrons and positrons to the energy deposit according to the initial kinetic energy distribution in an air shower has been studied elsewhere [23]. Only 10% of the energy deposit stems from particles with energies less than 0.1 MeV. Particles with energies between 0.1 and 10 MeV contribute 35%, between 10 and 100 MeV also 35%, and between 100 and 1000 MeV 17%. The remaining 3% originate from particles of energy above 1000 MeV. Several experiments have recently started to measure the proportionality of fluorescence yield to energy deposit. So far none of the results on the energy dependence is absolutely calibrated, thus a direct comparison is difficult. First relative results seem to confirm the expected correlation in different energy regions, see e.g. at about 1 MeV Nagano et al. [24], between 50 and 420 MeV Bohacova et al. [25], and at 28.5 GeV Belz et al. [26].

Depending on their initial energy, EAS particles produce secondary electrons of various lower energies. These can excite the  $N_2$  but they may also suffer an *attachment process*: if, on their way from the production site to the  $N_2$  molecules, the secondary electrons encounter a strong electronegative pollutant (e.g.  $O_2$ ,  $H_2O$ ,  $CO_2$ ,  $H_2$ ,  $Xe$ ,  $CH_4$  which are trace gases in the atmosphere), they are attached to this pollutants and cannot excite the  $N_2$  molecules anymore [13]. This process is beyond the scope of this paper.

### 2.1. Mathematical description

The existing results of fluorescence yield measurements show quite large differences. Furthermore, the data have to be applied to air shower reconstruction procedures. While secondary particles of EAS traverse from high to low altitudes, they encounter continuously changing atmospheric conditions. Additionally, the atmospheric conditions vary from day to day with the largest differences between the seasons summer and winter at the sites of all existing air shower experiments. The aim of the calcula-

tions shown here is to cross-check the laboratory measurements with the current understanding of the processes in the atmosphere, show possible sources of uncertainties, and provide an easy way to account for varying atmospheric conditions in EAS measurements.

The quantum efficiency of fluorescence can be defined as rate of de-excitation via radiation

$$\frac{\text{rate of de-excitation via radiation}}{\text{total rate of de-excitation}} = \frac{\tau_c}{\tau_0 + \tau_c}, \quad (4)$$

where the rate of de-excitation is proportional to the reciprocal of the life time. The mean life time of the radiative transition to any lower state is  $\tau_0$  and to collisional quenching  $\tau_c$ . The collisional quenching can be described by kinetic gas theory. The molecules, in the case of air, move with velocities following the Maxwell–Boltzmann distribution which is strongly correlated with gas temperature. As a good approximation, the collision rate depends on the mean velocity of molecules  $\bar{v} = \sqrt{\frac{8kT}{\pi M}}$ . The resulting mean life time due to collisional quenching is the ratio of the mean free path, in this case for molecules of one type moving with roughly the same velocity, and the mean velocity:

$$\begin{aligned} \tau_c &= \left( \sqrt{2} \cdot \rho_n \cdot \sigma_{NN} \cdot \bar{v} \right)^{-1} \\ &= \sqrt{(\pi M/kT)} \cdot (4\rho_n \cdot \sigma_{NN})^{-1}, \end{aligned} \quad (5)$$

where  $\rho_n$  is the particle number density,  $\sigma_{NN}$  the collisional cross-section between nitrogen molecules,  $T$  the temperature,  $k$  the Boltzmann constant, and  $M$  the molecular mass. Now the pressure-dependent fluorescence efficiency can be written as

$$\varepsilon_\lambda(p, T) = \frac{\varepsilon_\lambda^0}{1 + (p/p'_{v'})} = \frac{n \cdot E_\gamma}{E_{\text{dep}}}, \quad (6)$$

with  $\varepsilon_\lambda^0$  being the fluorescence efficiency at wavelength  $\lambda$  without collisional quenching,  $n$  denoting the number of photons,  $E_\gamma$  the energy of a single photon with the corresponding wavelength,  $E_{\text{dep}}$  the deposited energy in the observed medium, and  $p/p'_{v'} = \tau_{0,v'}/\tau_{c,v'}$ . The pressure  $p$  is that of the observed medium (e.g. air),  $p'_{v'}$  is a reference pressure at which  $\tau_0$  is equal to  $\tau_c$ .  $\tau_{0,v'}$  and  $\tau_{c,v'}$  are the mean life times for excitation level  $v'$ . Applying actual atmospheric conditions, with air taken to be a two-component gas, the relation between  $p$  and  $p'_{v'}$  can be written as

$$\begin{aligned} \frac{p}{p'_{v'}} &= \tau_{0,v'} \cdot \left( \frac{1}{\tau_{NN,v'}(\sigma_{NN,v'})} + \frac{1}{\tau_{NO,v'}(\sigma_{NO,v'})} \right) \\ &= \frac{\tau_{0,v'} p_{\text{air}} \cdot N_A}{R \cdot T} \cdot \sqrt{\frac{k T N_A}{\pi}} \cdot \left( 4 \cdot C_v(N_2) \cdot \sigma_{NN,v'} \sqrt{\frac{1}{M_{m,N}}} \right. \\ &\quad \left. + 2 \cdot C_v(O_2) \cdot \sigma_{NO,v'} \sqrt{2 \left( \frac{1}{M_{m,N}} + \frac{1}{M_{m,O}} \right)} \right), \end{aligned} \quad (7)$$

with Avogadro's number  $N_A$ , the masses per mole for nitrogen  $M_{m,N}$  and oxygen  $M_{m,O}$ , the universal gas constant  $R$ , the cross-sections for collisional de-excitation for nitrogen–nitrogen  $\sigma_{NN,v'}$  and nitrogen–oxygen  $\sigma_{NO,v'}$ ,

<sup>1</sup> Radiative transition probabilities.

and the fractional part per volume  $C_v$  of the two gas components.

## 2.2. Input parameters

To estimate the fluorescence efficiency with these equations, several parameters have to be obtained from measurements and/or calculations. Most important is the fluorescence efficiency without collisional quenching  $\varepsilon_{\lambda}^0$ . An early compilation of elder measurements performed by Bunner [14] provides these values for 18 band systems of the 2P and for 1 band system of the 1N state of nitrogen in the wavelength region between 300 and 400 nm. In a more recent publication by Gilmore et al. [17], the Einstein coefficients  $A_{v'v''}$  of the 2P nitrogen state for the transitions from  $v' = 0 \dots 4$  to  $v'' = 0 \dots 21$  and the radiative life times  $\tau_{0,v'}$  for  $v' = 0 \dots 4$  are given. For the 1N nitrogen state, the Einstein coefficients  $A_{v'v''}$  for the transitions from  $v' = 0 \dots 10$  to  $v'' = 0 \dots 21$  and the radiative life times  $\tau_{0,v'}$  for  $v' = 0 \dots 10$  are listed. The intensity of a transition could be calculated by  $N_{v' \rightarrow v''} = \tau_{0,v'} \cdot A_{v'v''} \cdot N_{v'}^*$ , where  $N_{v'}^*$  is the number of excited states. Since this number is unknown, a relative fluorescence efficiency is calculated by multiplying the Einstein coefficients with the radiative life times and a *relative apparent excitation cross-section*  $Q_{\text{app}}$  [27]. The *apparent excitation cross-sections* are the sum of the optical emission cross-sections over  $v''$  for a given  $v'$ . The excitation cross-sections are called apparent, because they represent the sum of direct excitation and cas-

cares from higher levels down to that particular one. The  $Q_{\text{app}}$  values are derived from the *apparent excitation cross-sections* by normalizing the value for  $v' = 0$  to unity of the electronic state. Values are given in the publication by Fons et al. [27] for the 2P band system of nitrogen for  $v' = 0 \dots 4$  and for the 1N band system for  $v' = 0 \dots 3$  in Stanton and St. John [28].

The relative fluorescence efficiency can then be normalized for each electronic state to, e.g., the most prominent band. For the 2P system of nitrogen, it is the (0–0) band with a wavelength of 337.1 nm, and for the 1N system it is again the (0–0) band with the corresponding wavelength of 391.4 nm. In our calculations, the efficiency values for these wavelengths as given in Bunner [14] are chosen.

In the following the fluorescence efficiencies are calculated for the bands of the 2P system. They dominate the fluorescence light emission in the atmosphere due to excitations caused by EAS. The fluorescence efficiencies labeled with  $\varepsilon_{\lambda, \text{G-F}}$  are obtained by applying the Einstein coefficients given by Gilmore et al. and the relative apparent excitation cross-sections from Fons et al. The values used within this paper are listed in Table 1.

Further parameters in the upper equations are the deactivation constants which are the radiative life time  $\tau_{0,v'}$  and the collisional cross-section between nitrogen and nitrogen molecules  $\sigma_{\text{NN},v'}$  and between nitrogen and oxygen molecules  $\sigma_{\text{NO},v'}$ . The values for  $\tau_{0,v'}$  obtained by Gilmore et al. are listed in Tables 1 and 3. Bunner provides collisional cross-sections and radiative life times for the most

Table 1  
Constants for the fluorescence efficiency  $\varepsilon_{\lambda}^0$  of the 2P system of nitrogen

Band ( $v'-v''$ )	Wavelength $\lambda$ (nm)	$\varepsilon_{\lambda, \text{Bunner}}^0$ (%)	Gilmore et al. [17]		Fons et al. [27] $Q_{\text{app}}$	$\varepsilon_{\lambda, \text{G-F}}^0$ (%)
			$A_{v'v''}$ (1/s)	$\tau_{0,v'}$ (s)		
2P (0–0)	337.1	.082	1.31E7	3.71E–8	1	.082
2P (0–1)	357.7	.0615	8.84E6	3.71E–8	1	.0553
2P (0–2)	380.5	.0213	3.56E6	3.71E–8	1	.0223
2P (1–0)	315.9	.050	1.19E7	3.75E–8	0.7	.0527
2P (1–1)	333.9	.0041	5.87E5	3.75E–8	0.7	.0026
2P (1–2)	353.7	.029	5.54E6	3.75E–8	0.7	.0245
2P (1–3)	375.5	.0271	4.93E6	3.75E–8	0.7	.0218
2P (1–4)	399.8	.016	2.43E6	3.75E–8	0.7	.0108
2P (2–1)	313.6	.029	1.01E7	3.81E–8	0.26	.0169
2P (2–2)	330.9	.002	7.99E5	3.81E–8	0.26	.0013
2P (2–3)	350.0	.004	1.71E6	3.81E–8	0.26	.0029
2P (2–4)	371.0	.010	4.04E6	3.81E–8	0.26	.0068
2P (2–5)	394.3	.0064	3.14E6	3.81E–8	0.26	.0052
2P (3–2)	311.7	.005	5.94E6	3.90E–8	0.081	.0032
2P (3–3)	328.5	.0154	2.85E6	3.90E–8	0.081	.0015
2P (3–4)	346.9	.0063	1.15E5	3.90E–8	0.081	.0001
2P (3–5)	367.2	.0046	2.35E6	3.90E–8	0.081	.0013
2P (3–6)	389.5	.003	3.00E6	3.90E–8	0.081	.0016
2P (4–3)	310.4	–	3.02E6	4.04E–8	0.041	.0008
2P (4–4)	326.8	–	3.71E6	4.04E–8	0.041	.0010
2P (4–5)	344.6	–	1.24E5	4.04E–8	0.041	.0000
2P (4–6)	364.2	–	9.98E5	4.04E–8	0.041	.0003
2P (4–7)	385.8	–	2.33E6	4.04E–8	0.041	.0007

Table 2  
Deactivation constants for air in the lower atmosphere

	Bunner [14]			Morozov et al. [29]		
	$\sigma_{\text{NO}}$ (m <sup>2</sup> )	$\sigma_{\text{NN}}$ (m <sup>2</sup> )	$\tau_0$ (s)	$\sigma_{\text{NN}}$ (m <sup>2</sup> )	$\sigma_{\text{N vapor}}$ (m <sup>2</sup> )	$\tau_0$ (s)
1N $\nu = 0$	13E–19	4.37E–19	6.58E–8	–	–	–
2P $\nu = 0$	2.1E–19	1.0E–20	4.45E–8	1.82E–20	8.53E–19	4.17E–8
$\nu = 1$	5.0E–19 <sup>a</sup>	3.5E–20	4.93E–8	3.77E–20	8.04E–19	4.17E–8
$\nu = 2$	7.0E–19 <sup>a</sup>	8.8E–20	4.45E–8	–	–	–
$\nu = 3$	8.0E–19 <sup>a</sup>	1.2E–19	6.65E–8	–	–	–

<sup>a</sup> This value is determined by the given results of [14] and not given in the original publication.

prominent band systems of nitrogen, see Table 2. Recent measurements by Morozov et al. [29] were performed for the 2P  $\nu' = 0, 1$  band systems, see also Table 2. In further calculations presented in this article, labeled with *Morozov*, the values from Bunner are replaced by the newer data by Morozov et al. were available.

No collisional cross-sections are available for the first-negative system of nitrogen for higher excitation levels than the (0–0) band. For an estimation of higher level contributions, one can assume that the collisional cross-section between the ionized nitrogen molecule and further nitrogen and oxygen molecules are equal to that of the (0–0) transition. Since the collisional cross-section usually increases for higher excitations, this is an assumption which gives an upper bound on the fluorescence light from these levels. The relative fluorescence yields for the 1N bands are estimated with the same method as already used for 2P, however, applying the parameters given in Gilmore et al. and Stanton and St. John (see  $\varepsilon_{\lambda, \text{G-St}}^0$  in Table 3). Even under these conditions, the 1N (1–0) and 1N (1–1) transitions add up to less than 1% to the total fluorescence yield between 300 and 400 nm at sea level in the US Standard Atmosphere. Higher excitations give even smaller contributions. Therefore, we will only consider the (0–0) transition of the 1N band and neglect the higher excitations.

The calculation introduced in Section 2.1 together with the  $\varepsilon_{\lambda, \text{Bunner}}^0$  and the deactivation constants from *Morozov* is used as reference model in this paper. It benefits from the completeness of the Bunner data and from the accuracy of the measurements from Morozov et al.

### 3. Comparison with measurements

Wavelength-dependent results of fluorescence yield measurements have been provided in three publications [14,30,31]. Bunner lists several intermediate values:  $\varepsilon_{\lambda}^0$ ,  $\varepsilon_{\lambda}^{\text{s.l.}}(p, T)$  in %, and the fluorescence efficiency  $\varepsilon_{E_{\text{dep}}}^{\text{s.l.}}$  in units of photons/MeV of deposited energy which is  $\varepsilon_{\lambda}^{\text{s.l.}}(p, T) \cdot (\lambda/hc)$  at sea level (s.l.). The values for  $\varepsilon_{\lambda}^{\text{s.l.}}(p, T)$  and  $\varepsilon_{E_{\text{dep}}}^{\text{s.l.}}$  given explicitly in [14] are not reproduced by the calculations shown here, see Table 4. Possible reasons are rounding uncertainties by Bunner or the use of deviating numbers for variables concerning air conditions. Davidson and O’Neil [31] list results for  $\varepsilon_{\lambda}^{\text{s.l.}}(p, T)$  for wavelengths above 320 nm. It should be mentioned that the results in [31] are given for  $p = 800$  hPa. The increase of the total fluorescence yield between 300 and 400 nm from sea level with  $p = 1013$  hPa to approximately 2 km a.s.l. with  $p = 800$  hPa amounts to about 2%. Nagano et al. report directly the values for  $\text{FY}_{\lambda}$  at sea level for 0.85 MeV electrons [30], however, only 10 contributing emission bands are listed. For comparing the results of all authors, 0.85 MeV electrons are chosen as exciting particles, so the ionization energy deposit is  $dE/dX = 0.1677$  MeV/kg m<sup>–2</sup> [24]. It is assumed that the fluorescence yield is proportional to the energy deposit as discussed in Section 2. Air is taken to be a composition of 78.8% N<sub>2</sub> and 21.1% O<sub>2</sub> per volume [24]. The resulting fluorescence yield can be written as

$$\text{FY}_{\lambda} = \varepsilon_{\lambda}(p, T) \cdot \frac{\lambda}{hc} \cdot \frac{dE}{dX} \cdot \rho_{\text{air}} \left[ \frac{\text{photons}}{\text{m}} \right]. \quad (9)$$

Table 3  
Constants for the fluorescence efficiency  $\varepsilon_{\lambda}^0$  of the 1N system of nitrogen

Band ( $\nu' - \nu''$ )	Wavelength $\lambda$ (nm)	$\varepsilon_{\lambda, \text{Bunner}}^0$ (%)	Gilmore et al. [17]		Stanton and St. John [28] $Q_{\text{app}}$	$\varepsilon_{\lambda, \text{G-St}}^0$ (%)
			$A_{\nu' \nu''}$ (1/s)	$\tau_{0, \nu'}$ (s)		
1N (0–0)	391.4	.33	1.14E7	6.23E–8	1	0.33
1N (1–0)	358.0	–	5.76E6	6.20E–8	0.117	0.0193
1N (1–1)	388.2	–	4.03E6	6.20E–8	0.117	0.0135
1N (2–0)	330.5	–	9.02E5	6.19E–8	0.009	0.0002
1N (2–1)	356.1	–	7.88E6	6.19E–8	0.009	0.0021
1N (2–2)	385.5	–	9.27E5	6.19E–8	0.009	0.0003
1N (3–1)	329.6	–	2.08E6	6.23E–8	0.004	0.0002
1N (3–2)	354.6	–	8.09E6	6.23E–8	0.004	0.0009

Table 4  
Fluorescence yield at sea level in the US Standard Atmosphere

Wavelength $\lambda$ (nm)	FY $_{\lambda}^{s,l}$ (photons/m) measurements from			FY $_{\lambda}^{s,l}$ (photons/m) calculations with		
	Bunner [14]	Davidson and O'Neil [31]	Nagano et al. [30]	$\epsilon_{\lambda,Bunner}^0$ , Table 2 – Bunner	$\epsilon_{\lambda,Bunner}^0$ , Table 2 – Morozov	$\epsilon_{\lambda,G-F}^0$ , $\sigma_{N_x}$ , Morozov, $\tau_{0,Gilmore}$
310.4	– <sup>a</sup>	– <sup>b</sup>	– <sup>a</sup>	–	–	0.001
311.7	0.008	– <sup>b</sup>	– <sup>a</sup>	0.009	0.009	0.010
313.6	0.090	– <sup>b</sup>	– <sup>a</sup>	0.094	0.094	0.064
315.9	0.224	– <sup>b</sup>	0.549	0.240	0.279	0.326
326.8	– <sup>a</sup>	– <sup>a</sup>	– <sup>a</sup>	–	–	0.002
328.5	0.027	0.035	0.180	0.029	0.029	0.005
330.9	0.007	– <sup>a</sup>	– <sup>a</sup>	0.007	0.007	0.005
333.9	0.019	– <sup>a</sup>	– <sup>a</sup>	0.021	0.024	0.017
337.1	0.887	1.173	1.021	1.169	1.108	1.242
344.6	– <sup>a</sup>	– <sup>a</sup>	– <sup>a</sup>	–	–	0.000
346.9	0.012	0.015	– <sup>a</sup>	0.012	0.012	0.000
350.0	0.014	0.013	– <sup>a</sup>	0.014	0.014	0.012
353.7	0.146	0.188	0.130	0.156	0.181	0.170
357.7	0.707	0.889	0.799	0.931	0.882	0.889
364.2	– <sup>a</sup>	– <sup>a</sup>	– <sup>a</sup>	–	–	0.001
367.2	0.009	0.012	– <sup>a</sup>	0.010	0.010	0.005
371.0	0.037	0.047	– <sup>a</sup>	0.038	0.038	0.030
375.5	0.150	0.187	0.238	0.155	0.180	0.160
380.5	0.261	0.328	0.287	0.343	0.325	0.381
385.8	– <sup>a</sup>	– <sup>a</sup>	– <sup>a</sup>	–	–	0.001
389.4	0.006	– <sup>a</sup>	– <sup>a</sup>	0.007	0.007	0.006
391.4	0.281	0.454	0.302	0.315	0.315	–
394.3	0.025	0.032	0.063	0.026	0.026	0.025
399.8	0.090	0.119	0.129	0.097	0.113	0.085
Sum of $\lambda = (300–400)$ nm	3.001	3.490 <sup>b</sup>	3.698	3.672	3.653	3.438 <sup>c</sup>
Sum of all Nagano-wavelengths	2.798	3.405 <sup>b</sup>	3.698	3.460	3.438	3.283 <sup>c</sup>
Sum of all Nagano-wavelengths above 320 nm	2.574	3.405	3.149	3.221	3.159	2.957 <sup>c</sup>
Sum of all Nagano-wavelengths above 320 nm and without 391.4 nm	2.293	2.951	2.847	2.906	2.844	2.957

For comparing the results of all authors, 0.85 MeV electrons are chosen as exciting particles, so the ionization energy deposit is 0.1677 MeV/kg m<sup>–2</sup>. See text for details.

<sup>a</sup> This transition has not been measured.

<sup>b</sup> Only measurements above 320 nm.

<sup>c</sup> Without 1N band system.

A comparison of the obtained FY $_{\lambda}$  values at sea level in the US Standard Atmosphere (US-StdA) [32,1] is shown in Table 4 and illustrated in Fig. 1.

The total fluorescence yield reported by Bunner directly in [14] is much lower than the other measurements and calculations. The total value from Davidson and O'Neil is higher by 6.8% for wavelengths above 320 nm as compared to our model for the same wavelength region. The calculations shown here applying  $\epsilon_{\lambda,Bunner}^0$  reproduce the measured values from Nagano et al. very accurately and the partly differing deactivation constants from Bunner and Morozov et al. do not affect the final result much. However, this holds only for the comparison of the whole wavelength region between 300 and 400 nm. One difficulty in the measurements is the treatment of interference filters which have

a bandwidth of about 10 nm [30]. The 10 contributions of Nagano et al. are given after subtracting additional contributions by smaller emissions within one filter region. Thus, for a direct comparison, one has to take into account only the 10 wavelengths reported in [30] and in this case, the calculations with  $\epsilon_{\lambda,Bunner}^0$  differ by approximately –7%. For a detailed comparison of each individual band system, see Fig. 2.

The measurements from Nagano et al. show two contributions which are considerably larger than all other data for those band systems at 315.9 and 394.3 nm. The largest relative difference occurs at the wavelength 328.5 nm where the value measured by Nagano et al. is higher by 512% compared to the preferred calculation presented here. However, the absolute contribution of this band emission

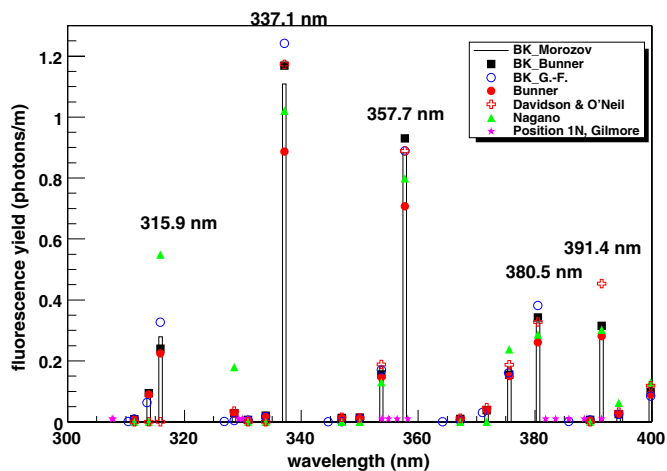


Fig. 1. Fluorescence yield spectra of several calculations and measurements for 0.85 MeV electrons as exciting particles. The bars indicate the preferred calculation presented in this article. All calculations are labeled with “BK\_name”, where *name* indicates the authors of the input parameters. Pink stars indicate the positions of possible contributions of the 1N system beyond the 1N (0–0) transition. (For color interpretation of Figs. 1, 2, 4 and 5 the reader refers to web version of this article.)

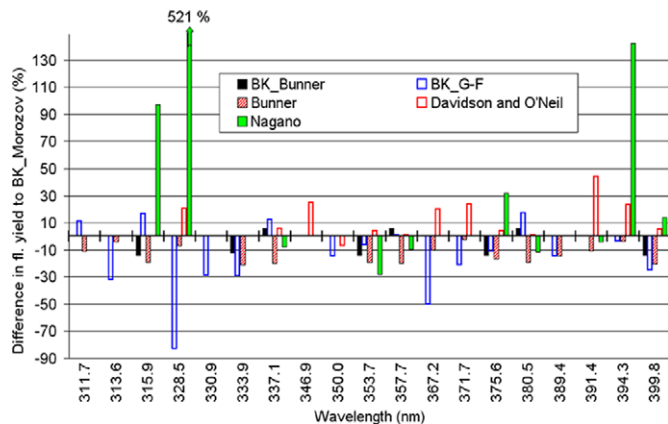


Fig. 2. Relative comparison of 19 band systems of the calculation preferred in this article with measurements and further calculations. The absolute fluorescence yield of these contributions can be seen in Fig. 1 with the same marking.

is only of minor importance for the entire wavelength region between 300 and 400 nm.

The calculations based on the Einstein coefficients given by Gilmore et al. lead to typically 20–30% lower fluorescence yield than our preferred calculation. Interestingly, the band emission at 328.5 nm, which is very bright in the measurements by Nagano et al., is much lower in the calculations using Gilmore et al. combined with Fons et al. data than in our model. These uncertainties might be caused by possible contributions from the 1N system, see Fig. 1 or Table 3.

Hirsh et al. [33] have performed measurements for the 1N (0–0) band system of nitrogen. They found a value for the fluorescence efficiency  $\epsilon_{391.4\text{nm}}^0$  of 0.475% which is considerably higher than the value given by Bunner, see

Table 1. Additionally, the collisional cross-section of nitrogen with nitrogen and nitrogen with oxygen have been investigated [33]. The values are  $\sigma_{\text{NN}} = 6.5 \times 10^{-19} \text{ m}^2$  and  $\sigma_{\text{NO}} = 10.9 \times 10^{-19} \text{ m}^2$ . Calculating the fluorescence yield for a 0.85 MeV electron with these parameters, the value at sea level in the US Standard Atmosphere amounts to 0.377 photons/m. A comparison of this number with the entries in Table 4 shows that  $\text{FY}_{391.4\text{nm}}$  measured by Hirsh et al. is larger than our calculation by 20%, larger than measurements from Nagano et al. by 25%, and larger than measurements published by Bunner even by 34%. Only measurements performed by Davidson and O’Neil result in a 17% higher  $\text{FY}_{391.4\text{nm}}$  than Hirsh et al.

Concluding, it can be stated that the calculations shown here provide a reasonable way of describing fluorescence emission in air while allowing for varying atmospheric conditions. This procedure can easily be implemented into air shower reconstruction programs. The overall agreement in the wavelength region between 300 and 400 nm with some measurements is already satisfying. However detailed, spectrally resolved comparisons reveal uncertainties in measurements and the understanding of the processes in air. Further investigations are necessary, as both atmospheric transmission and EAS detection are wavelength dependent. Also the dependence on altitude is different for the emission bands. Thus, for reconstructing the fluorescence emission of an EAS in the atmosphere from the measured photons, all these processes must be understood. It must be stressed that, for the EAS experiments, the uncertainties in fluorescence yield are directly linked to the uncertainties in the primary energy of cosmic rays.

It should also be mentioned that further fluorescence yield measurements, however without spectral resolution, can be found in literature. Kakimoto et al. provide a formula for calculating the fluorescence yield between 300 and 400 nm, which gives at sea level 3.275 photons/m [34]. This value is smaller by 10.3% compared to our preferred calculation. The HiRes Collaboration uses a value of about 5 photons/m per charged particle in an air shower [35]. For these charged particles, an average energy deposit of  $0.22 \text{ MeV/kg m}^{-2}$  is assumed [14], which leads to a corresponding fluorescence yield at s.l. of 3.811 photons/m for a 0.85 MeV electron. Assuming that the HiRes value refers to 5 km a.s.l., one would obtain 3.6–3.7 photons/m at s.l.

## 4. Dependence on atmospheric conditions

### 4.1. Altitude dependence

Firstly, the altitude dependence of the fluorescence efficiency  $\epsilon_{E_{\text{dep}}}$  in units of photons per MeV of deposited energy, as described in Section 3, will be shown. Eqs. (7) and (8) contain the altitude-dependent variables  $p$  and  $T$ . Combined with the deactivation constants, Table 2, a different altitude dependence for the 1N (391.4 nm) and 2P system (all other wavelengths) is expected, which is visualized in Fig. 3. Within the 2P system of nitrogen, there are

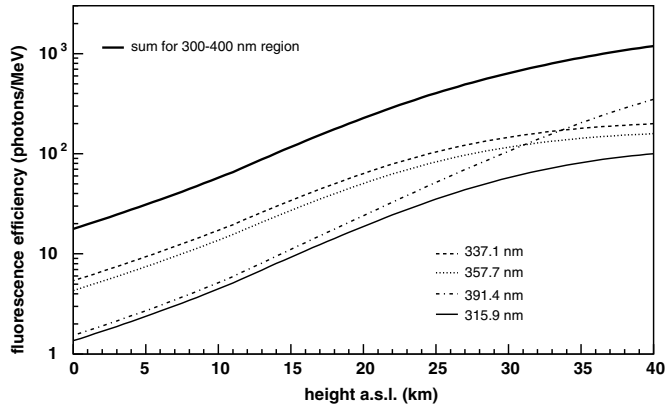


Fig. 3. Fluorescence efficiency profiles for different wavelengths in the US-StdA.

no differences in the altitude dependence for all emission bands belonging to the same excited state  $\nu'$  (e.g. 337.1 nm and 357.7 nm) and only small variations are between bands of different  $\nu'$  states (compare e.g. 315.9 nm from  $\nu' = 1$  and 337.1 nm from  $\nu' = 0$ ). With increasing altitude, the efficiency becomes larger due to lower rates of collisional quenching. This increase is largest for the 391.4 nm band. At sea level its contribution to the total spectrum amounts to 8.6%, at 20 km a.s.l. it is already 10.7%, and at 30 km a.s.l. 16.8%.

However, regarding EAS, the rate of emitted photons per meter traversed matter of the EAS is the observed variable which is the fluorescence yield  $FY_\lambda$ , Eq. (9). Via the altitude-dependent air density,  $\rho_{\text{air}}$ , the number of excitable nitrogen molecules and quenching partners are considered. For simplicity,  $FY_\lambda$  vs. altitude is shown in Fig. 4 for a 0.85 MeV electron. The most relevant altitude range for EAS is between ground and about 13 km a.s.l. For EAS with energies of about  $10^{19}$  eV, the shower reaches its max-

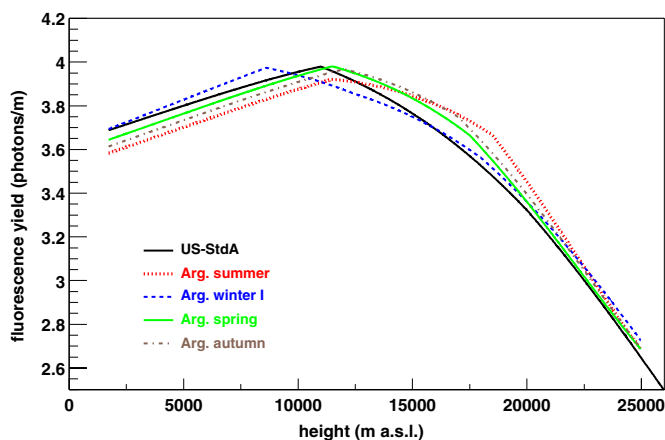


Fig. 4. Fluorescence yield profiles for a 0.85 MeV electron with vertical incidence in the US Standard Atmosphere and measured Argentine atmospheres as given in [1]. The given yield is a sum of all emitted photons between 300 and 400 nm calculated as described in Section 3 with  $\varepsilon_{\lambda, \text{Bunner}}^0$  and Table 2<sub>MOROZOV</sub>.

imum between 2 and 8 km a.s.l. depending on the type of the primary particle and the inclination angle of the EAS.

For example, for the Auger experiment, the field of view of a telescope covers an altitude range between 0.7 km and 12.5 km above the altitude of the Pierre Auger Observatory, 1.4 km a.s.l., at a distance of 20 km. The fluorescence yield plotted in Fig. 4 is a sum of all emitted photons between 300 and 400 nm calculated as described in Section 3 with  $\varepsilon_{\lambda, \text{Bunner}}^0$  and Table 2<sub>MOROZOV</sub>. Additionally to the altitude dependence, also the seasonal dependence for actual atmospheres as obtained at the southern site of the Pierre Auger Observatory [1] can be seen in Fig. 4. From ground level to altitudes around 10 km, the fluorescence yield increases slowly. Above 10 km, the yield decreases disclosing the sensitivity to temperature and pressure variations. During winter I, the lower temperatures compared to the other atmospheric models below 9 km a.s.l. induce a higher fluorescence yield. Up to 17 km, the temperatures are comparatively high leading to a reduced fluorescence yield. During spring, summer, and autumn the temperatures are higher than in the US-StdA, therefore the fluorescence yield is decreased mostly in summer. Above 15 km a.s.l., the very low temperatures during summer result in a very high emission. The differences of  $FY_\lambda$  for the Argentine seasons compared to the US-StdA are well below  $\pm 5\%$ . At the altitude of the Auger detectors, 1.4 km a.s.l., the increase in fluorescence yield during winter I is negligible, however the decrease in summer amounts to 2.9%. At  $\approx 8.5$  km, the differences of summer and winter I to the US-StdA are of the same size but with opposite signs. In winter I,  $FY_\lambda$  is 1.5% higher than in the US-StdA, and in summer 2.2% lower. More than +4% difference from Argentine summer to the US-StdA emerges above 16.5 km a.s.l. Similar seasonal variations in  $FY_\lambda$  are also valid for other EAS experiments since similar atmospheric conditions have been found at different places [1,36].

The calculated altitude dependence can be compared with parameterizations given by authors from fluorescence emission experiments. The functional forms of these parameterizations are inspired by the same equations as introduced in Section 2.1 [30,34]:

$$FY_\lambda^{[30]} = \frac{dE}{dX} \cdot \left( \frac{A_\lambda \rho}{1 + \rho B_\lambda \sqrt{T}} \right), \quad (10)$$

$$FY_{300-400 \text{ nm}}^{[34]} = \frac{dE}{dX} \cdot \rho \left( \frac{A_1}{1 + \rho B_1 \sqrt{T}} + \frac{A_2}{1 + \rho B_2 \sqrt{T}} \right). \quad (11)$$

While Nagano et al. [30] list  $A$  and  $B$  parameters for each of their 10 wavelengths between 300 and 400 nm, Kakimoto et al. [34] just provide one set of parameters  $A_{1,2}$  and  $B_{1,2}$  for the total fluorescence yield between 300 and 400 nm. Both approaches predict similar height dependences, see Fig. 5. To work out the difference due to the altitude dependence, the profiles can be shifted so that all curves start with the same value at sea level. Then the parameterization by Nagano et al. agrees very well with the calculation introduced in this paper. Up to 14 km,

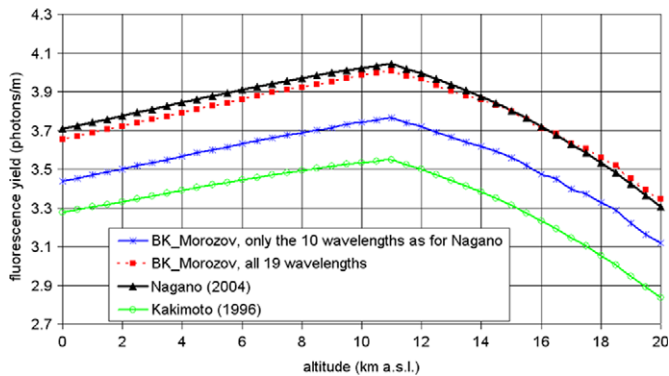


Fig. 5. Fluorescence yield profiles for a 0.85 MeV electron in the US-StdA. Comparison of the altitude dependence calculated by the described method with two further parameterizations.

the discrepancy is below 1%, increasing up to 2.9% at 20 km a.s.l. The simplified parameterization given by Kakimoto et al. disagrees already above 6.5 km with the calculations shown here by more than 1%. The difference increases up to 4% at 20 km a.s.l.

#### 4.2. Humidity dependence

All calculations and measurements shown above are based on dry air conditions. However, in actual atmospheric conditions, there is sometimes a considerable fraction of water vapor. Thus, the effect of quenching due to water vapor has to be investigated. Fluorescence emission by water vapor is not expected.

Our first calculations are based on Eq. (8) in which an additional term is inserted to account for the collisions between nitrogen and water vapor molecules. The experimental determination of collisional cross-sections between nitrogen and water vapor, which are needed in that equation, is very difficult. Two experiments have recently begun to investigate the effect of water vapor [29,37].

The effect of quenching due to water vapor has been studied in our preferred calculation for the 337.1 nm emission band. Applying the parameters from Table 2 by Morozov et al. and assuming 100% relative humidity, the emission at sea level is reduced by approximately 20%, at 4 km a.s.l. by roughly 5%, and at 8 km a.s.l. just by 0.3%. Since fluorescence telescopes typically operate only during “good weather” periods, this decrease in fluorescence yield should be considered as an upper limit. For realistic atmospheric conditions, a reduction of about 5–10% near ground and 1–3% at 4 km a.s.l. can be expected.

### 5. Summary and conclusion

EAS experiments applying the fluorescence technique measure the light emission in air induced by charged particles, mainly electrons and positrons. The detected light track is converted into a longitudinal shower profile and finally to the total energy of the primary particle of the

EAS. Therefore, the fluorescence light yield has to be known precisely including spectral resolution and dependence of atmospheric conditions.

The results on fluorescence yield which can be found in literature differ considerably. Most important are the fluorescence efficiency of the contributing band systems of nitrogen, but also the radiative life times and the collisional cross-sections of nitrogen with nitrogen and nitrogen with oxygen have to be known. Up to now, a thorough understanding of the energy-dependent excitation processes of the different nitrogen states is missing. First studies can be found in Blanco and Arquerros [38].

In this article, an atmosphere-dependent description of the fluorescence light emission in air has been presented. The different contributions of the 2P and 1N band systems of nitrogen have been calculated in detail. The calculations are based on several parameter sets and have been compared with fluorescence yield measurements performed by several authors. The calculations reproduce some results of measurements well, while other data are off by more than 10% regarding the total yield between 300 and 400 nm. The differences for individual emission bands are much larger.

The variation of the fluorescence yield with changing atmospheric conditions has only been studied by a few authors. Generally, it is assumed that the main reduction of light emission is due to collisional quenching. The calculation of altitude-dependent profiles of  $FY_\lambda$  presented here agree within 4% with parameterizations of measurements.

Using the calculation and parameter set preferred in the article, a prediction of the influence of water vapor has been made. For realistic atmospheric conditions, an effect of about 5–10% near ground and less than 3% at altitudes around 4 km a.s.l. can be expected. Only lately experimental studies of the quenching rate of water vapor have been begun.

#### Acknowledgement

One of the authors (BK) is supported by the German Research Foundation (DFG) under contract No. KE 1151/1-1.

#### References

- [1] B. Keilhauer, J. Blümer, R. Engel, H.O. Klages, M. Risse, *Astropart. Phys.* 22 (2004) 249.
- [2] C.C. Jui et al. (HiRes Collab.), in: *Invited Rapporteur and Highlight Papers, Proceedings of the 26th International Cosmic Ray Conference (Salt Lake City), 2000*, p. 370.
- [3] A. Etchegoyen et al., FERMILAB-PUB-96-024. Available from: <<http://www.auger.org/admin/DesignReport/>> 1996.
- [4] J. Blümer (Pierre Auger Collab.), *J. Phys. G29* (2003) 867.
- [5] J. Abraham et al. (Pierre Auger Collab.), *Nucl. Instrum. Methods Phys. Res. A523* (2004) 50.
- [6] M. Fukushima et al. (TA Collab.). Available from: <<http://www-ta.icrr.u-tokyo.ac.jp/TA/>> 2000.
- [7] M. Fukushima, *Prog. Theor. Phys. Suppl.* 151 (2003) 206.
- [8] P. Sommers et al. (Pierre Auger Collab.), in: *Proceedings of the 29th International Cosmic Ray Conference, Pune, India, 2005*.

- [9] AGASA Collaboration. Available from: <<http://www-akeno.icrr.u-tokyo.ac.jp/AGASA/resuls.html>> 2004.
- [10] R.U. Abbasi et al. (HiRes Collab.), *Phys. Rev. Lett.* 92 (2004) 151101.
- [11] R. Engel, H. Klages, *C. R. Phys.* 5 (2004) 505.
- [12] W.R. Bennett Jr., J. Flint, *Phys. Rev. A* 18 (1978) 2527.
- [13] A.E. Grün, E. Schopper, *Z. Naturforsch.* 9a (1954) 134.
- [14] A.N. Bunner, *Cosmic Ray Detection by Atmospheric Fluorescence*, Ph.D. Thesis, Cornell University, Ithaca, NY, USA, 1967.
- [15] A. Morozov, R. Krücken, T. Ottenthal, J. Wieser, A. Ulrich, *Appl. Phys. Lett.* 86 (2005) 011502.
- [16] R.W. Nicholls, E.M. Reeves, D.A. Bromley, *Proc. Phys. Soc.* 74 (1959) 87.
- [17] F.R. Gilmore, R.R. Laher, P.J. Espy, *J. Phys. Chem. Ref. Data* 21 (1992) 1005.
- [18] H. Haken, H.C. Wolf, *Molekülphysik und Quantenchemie*, Springer Verlag, Berlin, 1998.
- [19] G. Herzberg, *Molecular Spectra and Molecular Structure: I. Spectra of Diatomic Molecules*, D. van Nostrand Company, New York, 1950.
- [20] J.T. Fons, J.S. Allen, R.S. Schappe, C.C. Lin, *Phys. Rev. A* 49 (1994) 927.
- [21] Y. Itikawa et al., *J. Phys. Chem. Ref. Data* 15 (1986) 985.
- [22] J.P. Santos, F. Parente, Y.-K. Kim, *J. Phys.* B36 (2003) 4211.
- [23] M. Risse, D. Heck, *Astropart. Phys.* 20 (2004) 661.
- [24] M. Nagano, K. Kobayakawa, N. Sakaki, K. Ando, *Astropart. Phys.* 20 (2003) 293.
- [25] M. Bohacova et al., in: *Proceedings of the 29th International Cosmic Ray Conference*, Pune, India, 2005.
- [26] J.W. Belz et al. (FLASH Collab.). Available from: <[astro-ph/0506741](mailto:astro-ph/0506741)> 2005.
- [27] J.T. Fons, R.S. Schappe, C.C. Lin, *Phys. Rev. A* 53 (1996) 2239.
- [28] P.N. Stanton, R.M. St. John, *J. Opt. Soc. Am.* 59 (1969) 252.
- [29] A. Morozov, R. Krücken, J. Wieser, A. Ulrich, *Eur. Phys. J. D* 33 (2005) 207.
- [30] M. Nagano, K. Kobayakawa, N. Sakaki, K. Ando, *Astropart. Phys.* 22 (2004) 235.
- [31] G. Davidson, R. O'Neil, *J. Chem. Phys.* 41 (12) (1964) 3946.
- [32] National Aeronautics and Space Administration (NASA), *US Standard Atmosphere 1976*, NASA-TM-X-74335, 1976.
- [33] M.N. Hirsh, E. Poss, P.N. Eisner, *Phys. Rev. A* 1 (1970) 1615.
- [34] F. Kakimoto et al., *Nucl. Instrum. Methods Phys. Res. A* 372 (1996) 527.
- [35] R.U. Abbasi et al. (HiRes Collab.), *Astrophys. J.* 622 (2005) 901.
- [36] B. Wilczynska et al., *Variation of atmospheric depth profile on different time scales*, in: *Proceedings of the 29th International Cosmic Ray Conference*, Pune, India, 2005, *Astropart. Phys.*, submitted for publication.
- [37] N. Sakaki, K. Kobayakawa, M. Nagano, Y. Watanabe, in: *Proceedings of the 29th International Cosmic Ray Conference*, Pune, India, 2005.
- [38] F. Blanco, F. Arqueros, *Phys. Lett. A* 345 (2005) 355.